Pyrazine Functionalized Ag(I) and Au(I)-NHC Complexes are Potential Antibacterial Agents

G. Roymahapatra[#,1], S.M. Mandal*[,#,2], W.F. Porto[3], T. Samanta[1], S. Giri[4], J. Dinda*[,1], O.L. Franco[3] and P.K. Chattaraj[4]

[1]*School of Applied Sciences, Haldia Institute of Technology, Haldia -721657, WB, India;* [2]*Central Research Facility, Indian Institute of Technology, Kharagpur, Kharagpur- 721302, WB, India;* [3]*Centro de Análises Proteômicas e Bioquímicas, Pós-Graduação em Ciências Genômicas e Biotecnologia UCB, Brasília-DF, Brazil;* [4]*Department of Chemistry, Centre for Theoretical Studies, Indian Institute of Technology Kharagpur, Kharagpur 721302, WB, India*

Abstract: Antimicrobial resistance is an ever-increasing problem throughout the world and has already reached severe proportions. Bacteria can develop ways to render traditional antibiotics ineffective, raising a crucial need to find new antimicrobials with novel mode of action. We demonstrate here a novel class of pyrazine functionalized Ag(I) and Au(I)-NHC complexes as antibacterial agents against human pathogens that are resistant to several antibiotics. Complete synthetic and structural studies of Au(I) and Ag(I) complexes of 2-(1-methylimidazolium) pyrimidinechloride (**L-1**), 2,6-bis(1-methylimidazol)pyrazinechloride (**L-2**) and 2,6-bis(1-methyl imidazol) pyrazinehexa-fluorophosphate (**L-3**) are reported herein. Chloro[2,6-bis(1-methyl imidazol)pyrazine]gold(I), **2b** and chloro [2,6-bis(1-methyl imidazol)pyrazine]silver(I), **2a** complexes are found to have more potent antimicrobial activity than other synthesized compounds and several conventionally used antibiotics. Complexes **2b** and **2a** also inhibit the biofilm formation by Gram-positive bacteria, *Streptococcus mutans* and Gram-negative bacteria, *Escherichia coli,* causing drastic damage to the bacterial cell wall and increasing membrane permeability. Complexes **2b** and **2a** strongly binds to both Lys and Dap-Type peptidoglycan layers, which may be the reason for damage to the bacterial cell wall. Theoretical studies of all the complexes reveal that **2b** and **2a** are more reactive than other complexes, and this may be the cause of differences in antibacterial activity. These findings will pave the way towards developing a new class of antibiotics against different groups of conventional antibiotic-resistant bacteria.

Keywords: Ag(I) and Au(I)-NHC complexes, antibacterial activity, biofilm eradication, peptidoglycan layer, CDFT.

INTRODUCTION

The increasing occurrence of microbial infections, rapid emergence of drug-resistance to conventional antibiotics and quick evolution through mutation are substantial threats to the control of microbial infection. Antimicrobial resistance is a serious problem today, and its global spread not only undermines the continued effectiveness of antimicrobial drugs but also threatens global health security. Infections caused by antibiotics resistant organisms are also an epidemiological concern, as they may spread locally, regionally and globally through individual contact, poor sanitation, and travel or food chains [1]. Hence, there is an urgent need to discover and develop new antimicrobials with novel mechanisms to combat infectious diseases and save lives.

N-heterocyclic carbenes (NHCs) are defined as singlet-carbenes containing a divalent carbenic carbon with nitrogen atom in heterocycle [2-6]. Wanzlick [7-9] first proposed their existence and Arduengo *et al*. first isolated the free bottleneck NHC [10]. Thereafter, many advances have been made in the synthesis, characterization, and reactions of NHCs with diverse electronic and steric properties [2-3,6,11-13]. The development of stable N-heterocyclic carbene metal complexes has attracted increasing attention in metallopharmaceuticals, which play a significant role in therapeutic and diagnostic medicine. NHCs derived from the deprotonation of 1,3 di-substituted imidazolium salts, by appropriate external base, produce NHC complexes, which are stabilized through a "push-pull" mechanism [14-16]. The metal-NHC complexes are synthesized in different ways and one of the most convenient of these, which overcomes the difficulties of unstable free heterocyclic carbenes isolation, is the use of silver carbene complexes as carbene transfer reagents for the synthesis of other metal-NHC complexes [17]. The stability of Ag-NHC complexes is greatly enhanced by the addition of electron withdrawing groups on the 4 and 5 positions of the imidazole ring. Further, the synthesis of stable Au-NHC complex is directed one step from Ag-NHC complex [18-25].

Earlier NHCs were diversified by changing mostly C(4,5) and by N-substitution. So-called 'hybrid NHCs' appending pyridine, pyrimidine, pyrazole, oxazole and thiazole in the imidazoline system are well established [26-27]. Recently, much attention has been paid to NHC pincer-carbene complexes due to their excellent chelating effects and reactivities. In the literature only one report of pyrazine functionalized CNC-pincer NHC is available [28], and no studies on complex formation and biomedical applications are reported, which encouraged us to carry out the synthesis of pyrazine functionalized pincer NHCs-Ag and Au complexes and to analyze their antibacterial applications. Few metal-NHC complexes have been tested in medicinal applications, which created our interest in synthesizing a new class of compounds and investigating their biomedical activities. Hindi *et al*. (2009) [29] published an excellent review dealing with the medicinal applications of various transition metal-NHC complexes, including silver, gold, rhodium, ruthenium, and palladium. Panzner *et al*. (2009) [30] synthesized silver N-heterocyclic carbene derived from naturally occurring xanthine; furthermore, caffeine showed improved activity against clinical isolate, *Pseudomonas aeruginosa* M57-15. A series of methylated imidazolium salts with varying substituents on the C(4 and 5) positions of the imidazole ring were synthesized and reacted with silver acetate to afford water-stable silver N-heterocyclic carbene (NHC)- silver complexes [31]. These complexes also showed antimicrobial activity against cystic fibrosis and chronic lung infection pathogens (Hindi *et al*., 2008) [32]. Recently, benzyl-substituted NHC-silver acetate complexes [31] showed antibacterial activity against Gram-positive bacteria *Staphylococcus aureus*, and Gram-negative bacteria *Escherichia coli*. Ghosh and coworkers [33] used gold -NHC complex, [1-Benzyl-3-tert-butylimidazole-2-ylidene] AuCl and silver (NHC) complex, [1-Benzyl-3-tert-butylimidazole-2-ylidene] AgCl and tested their antimicrobial properties against *Bacillus subtilis* and *Escherichia coli*. Interestingly, both complexes exhibited significant antimicrobial activity against *B. subtilis* but had no effect against *E. coli*.

*Address correspondence to this author at the Central Research Facility, Indian Institute of Technology, Kharagpur, Kharagpur- 721302, WB, India; Tel: + 91-3222-282486, Fax: +91-3222-282481; E.mail: sm_crf@yahoo.com

[#]Authors also contributed equally to the experimental part.

0929-8673/12 $58.00+.00

In this study, we first report the antibacterial activity of pyrazine functionalized pincer NHC-Ag(I) and NHC-Au(I) complexes against antibiotics resistant human pathogens of both Gram-positive and Gram-negative bacteria, including their inhibitory effects on biofilm formation. Their synthesis, characterization, theoretical explanation and mode of action are analyzed in detail.

EXPERIMENTAL SECTION

Chemicals and Reagents

All the reagents 1-methylidazole,2,6-dichloropyrazine, 2-chloropyrimidine, Ag_2O, CuI, NH_4PF_6 were purchased from Sigma-Aldrich, UK, and were used without further purification. All manipulations were carried out under an open atmosphere unless otherwise stated. All the solvents were distilled over appropriate dry agents and N2-saturated prior to use. All the selected antibiotics tested in this study were purchased from HIMEDIA, India.

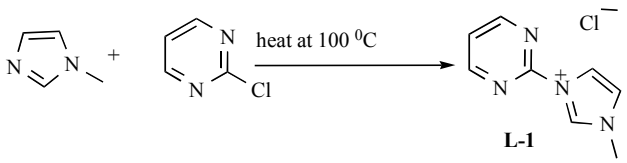

Scheme 1. The synthesis procedure of ligand **L-1**, 2- (1-methylimidazolium) pyrimidinechloride.

Synthesis of the Compounds

The pyrimidine functionalized proligand 1-methyl-3-pyrimidinechloride **(L-1),** 2,6-bis-[1-methylimidazol-2yl]pyrazinechloride **(L-2)** and 2,6-bis(1-methyl imidazolium-2yl) pyrazinehexafluorophosphate **(L-3)** and ligands derived compounds **(2a-3b)** were synthesized as shown in Schemes **1** and **2**. The details synthetic procedure was described in supplementary section. Microanalytical and mass spectrometry data of all synthesized complexes **2a-3b,** along with the pro-ligands were also described details in supplementary section. All spectra of the complexes were obtained on a Shimadzu UV-1601. ^{1}H and ^{13}C NMR spectra were recorded on Bruker 400 and 300 MHz spectrometers. Chemical shifts, d, are reported in ppm relative to the internal standard TMS for both ^{1}H and ^{13}C NMR. J values are given in Hz. Elemental analyses are performed using a Perkin-Elmer 2400 C elemental analyzer. The theoretically optimized structures of compounds were established using Gaussian G-03-E01 suit [42].

Antimicrobial Assay

Staphylococcus epidermidis NCIM2493, *Streptococcus mutans* MTCC890, *Escherichia coli* ATCC25922 and *Pseudomonas aeruginosa* ATCC27853 strains were used for this study. MIC values of all the synthesized compounds and tested antibiotics were determined according to CLSI guidelines [34]. The concentration of each compound used for the assay ranged from 1.0 to 1024 µg.mL^{-1}. MIC values were determined where no visible growth was observed. A range of concentration of each synthetic compound was added to sterile 96-well microtitre plates and the volume was made up to 250 µL/ well with Mueller-Hinton broth (MHB). Culture of individual strain was added to the mixtures to achieve a total inoculum load of ca. 10^5 cells/ well. Finally, microtitre plates were incubated at 37 °C for 18 h. Bacterial growth was measured by optical density at 600 nm using a Multiskan Spectrum spectrophotometer (model 1500; Thermo Scientific, Nyon, Switzerland) and the MIC value of each compound was determined by comparing the cell densities with wells where no compound was added as positive control and no bacterium with only compound was used as negative control to maintain the sterility. Each experiment was repeated four times.

Scanning Electron Microscopy (SEM)

Bacterial cells were harvested from the log phase of their growth; compounds were treated for 30 min and their MIC values determined. Immediately, the cells were washed three times with

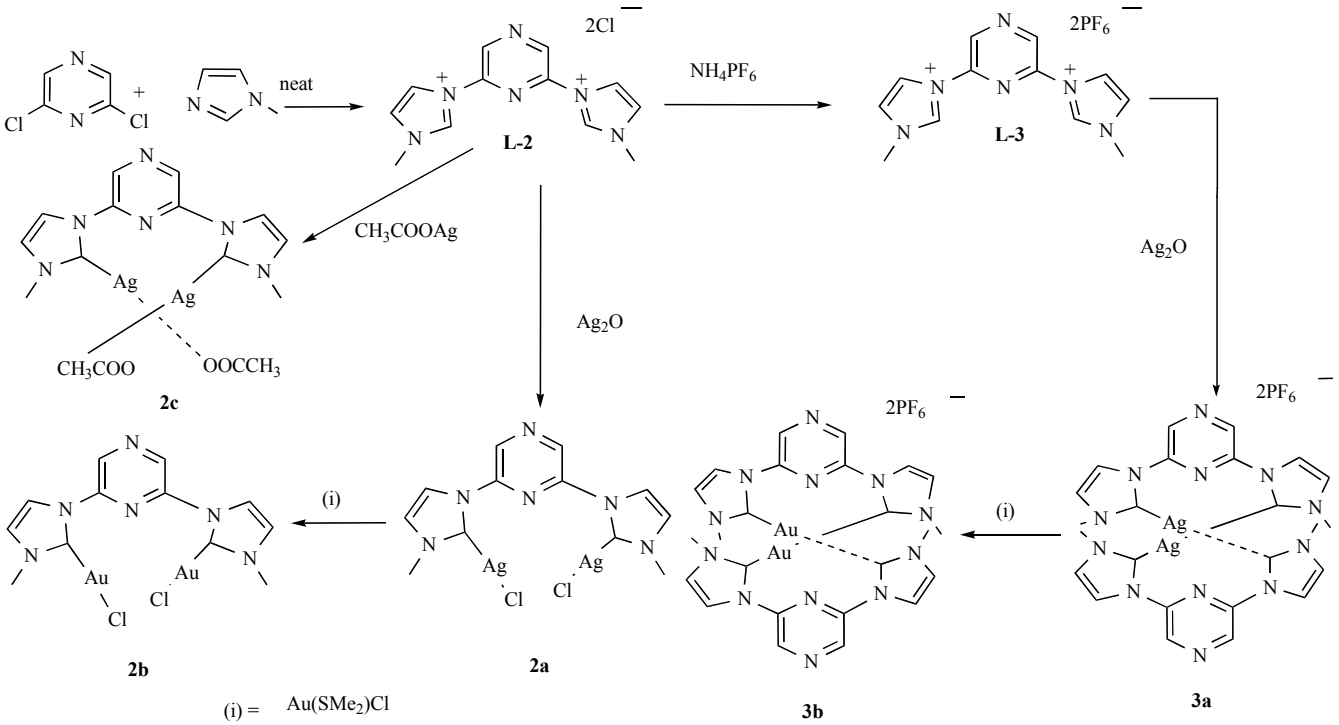

Scheme 2. The schematic diagram of the synthesis procedure of ligand, **L-2, L-3** and their derived compounds.

1X PBS. The cells were then resuspended in the same saline buffer and 5-10 µl of culture placed on the lysine-coated glass cover slip as drop-caste method. The fixed cells were dried and kept on a desiccator until use. Samples were then fixed onto a graphite stub and kept in an auto sputter coater (E5200, Bio-Rad) under low vacuum for gold coating up to 120 seconds. Surface morphology was studied by using a scanning electron microscope (JEOL JSM5800) with an accelerated voltage 5-20 kV.

Flow Cytometry Analysis

Membrane permeability and live/dead bacterial cell counts were determined by flow cytometry analysis following Mandal *et al* [35] after some modification and maintained the manufacturer's guidelines (LIVE/DEAD ® BacLight™ Bacterial Viability and Counting Kit, Invitrogen, India). BacLight stain contains both SYTO 9 and Propidium iodide (PI) dye, a unique combination to determine the live and dead cells and also useful for permeabilization monitoring of the cells. In brief, *S. epidermidis* was grown to mid log phase in MHB, washed three times with buffer (10 mM Tris, pH 7.4) and resuspended in buffer to obtain 2×10^8 CFU/ml bacterial suspension. The bacterial suspension was diluted to 10^5 CFU/mL in the same buffer. The cells were incubated with BacLight™ without compound, as negative control, and 4 $\mu g.mL^{-1}$ of fixed compound concentration was used for positive control. Cells were harvested at a regular 10 min interval from the starting of incubation in positive control experiment and up to 60 min. A FACS flow cytometer (FACS Caliber flow cytometer, Becton-Dickinson, USA) was used to obtain the data with a 488 nm wavelength of laser excitation. Data were analyzed by Cell QuestPro software attached to FACS Caliber.

Detection of Biofilm Formation and Minimum Biofilm Eradication Concentration Assay

Biofilm quantification was carried out using polystyrene crystal violet adherence assay as described previously by Croes *et al*. [36]. Briefly, overnight cultures in Trypticase Soy Broth (TSB) without dextrose were diluted until 10^8 CFU/mL in TSB containing 0.5% glucose was obtained. Bacterial inoculum (10^5 CFU/well) was added in the wells and incubated for 48 h allowed for biofilm formation. We have also grown the *S. mutans* biofilms on hydroxyapatite discs as described by Coenye *et al*. [37] and lyophilized saliva was coated after dissolved in adhesion buffer (1 mM CaCl2, 2 mM potassium phosphate, 50 mM KCl) at a concentration of 1.5 $mg.mL^{-1}$ as described previously [38]. The minimum biofilm eradication concentration was determined following Olson *et al*. [39]. The planktonic bacterial cells were washed twice using PBS (0.1 M). Individual wells of polystyrene plate containing sessile cells were filled with 200 **µ**L aliquots of TSB used as positive control, while for negative control only medium (without bacterial cells) was added to a new well and different concentrations (0-16 $\mu g.mL^{-1}$) of compound 2b and 2a in 200 **µ**L TSB were added to wells in duplicate for experiment. After 24 h, the medium was aspirated off from each well and washed with PBS (0.1 M). In order to quantify, 100 **µ**l crystal violet solutions (0.5% wt/vol) was added to separate replicate wells. After 15 min, the excess crystal violet was rinsed off by PBS solution. Finally, after drying the plates, bound crystal violet was retained by adding 100 **µ**l of 70% (vol/ vol) ethanol with 10% isopropyl alcohol (vol/ vol). Absorbance was measured spectrophotometrically at 590 nm (**A**590) and was proportional to biofilm biomass. All assays were performed in triplicate. Subsequently, the biofilm formations in different concentrations were visualized under fluorescence microscope (OLYMPUS IX 51, fitted with Evolution VF CCD Camera) by staining with LIVE/DEAD ® BacLight™ Bacterial stain (Invitrogen, India).

Hemolytic Assay

The hemocompatibility study was performed following the protocol by Mandal *et al*. [40]. In brief, RBC (from 6-week-old male BALB/c mice) suspension was added to HEPES-buffered saline (negative control), 1.0% Triton X-100 (positive control) and incubated with different concentration of **2a** and **2b** for 1h at 37°C. After incubation, the supernatants were transferred to a 96-well plate. Hemolytic activity was determined by measuring the absorption at 570 nm. Control samples of 0% lysis (in HEPES buffer) and 100% lysis (in 1% Triton X-100) were considered in the experiment. All assays were performed in triplicate. Hemolytic effect of each treatment was expressed as percent cell lysis relative to the positive control using the following formula: [(Abs_{570} of compounds)/ (Abs_{570} of positive control)] × 100.

Theoretical Calculations

The stability and reactivity of the ligands and associated complexes were analyzed with the help of conceptual density functional theory (CDFT)-based global and local reactivity descriptors. The CDFT-based reactivity descriptors like electronegativity ($\chi = (I + A)/2$, where I and A are ionization potential and electron affinity respectively) [41], hardness ($\eta = (I - A)$) [42] and electrophilicity ($\omega = \chi^2 / 2\eta$) [43], were calculated using standard formulae. All the ligands and complexes were optimized at B3LYP level of theory with the LANL2DZ basis set using Gaussian G-03-E01 suit [44]. We also optimized the ligands using different basis sets at the B3LYP level of theory to get an idea of the effect of basis sets on stability. In all cases we got the number of imaginary frequency values to be zero, which confirmed their existence at the minima on the potential energy surface. In order to determine the relative potential energy barriers (ΔE, indicating the energy difference between the highest and lowest energy conformers) of the different conformers of the complexes, these were calculated as a function of the tortional angle [45].

Molecular Docking

Firstly, the Lys-Type Peptidoglycan structure was obtained from PDB file 2EAX, Cho *et al*. [46] and visualized by PyMol 1.2r2, DeLano [47]. The structure of Dap-Type peptidoglycan was constructed by using Lys-Type atomic coordinates with the addition of a formic acid to the carbon ε from lysine by using PyMol. Molecular docking studies were theoretically performed by AutoDock Vina [48] and AutoDock Tools [49]. The grid box was set up in order to permit the interaction of ligands **2a** and **2b** to the whole peptidoglycan molecule. First, the grid box was set to the center of peptidoglycan molecules and then its size was set to 40, 22, 36, for X,Y and Z axis, respectively. Structures of **2a** and **2b** were set as flexible ligands by using default parameters of AutoDock Tools. Final models were analyzed on AutoDock Tools and PyMol. Theoretical affinity comparisons between compounds docked with different peptidoglycans were performed by counting the number of electrostatic interactions and also by the index of relative area contact (RAC). RAC is defined by the subtraction of peptidoglycan surface area from the complex surface area where a value of RAC equal to zero indicates total contact between two areas. This index is inversely proportional to contact area, which is calculated by using the solvent accessible surface areas.

Statistical Analysis

The results are presented as the mean ± the SD. The statistical significance of the experimental results was determined to one-way Student's t-test or one-way ANOVA followed by Dunnett's test.

Table 1. Determination of Minimum Inhibitory Concentration of Synthesized Compounds Against Gram-Positive and Gram-Negative Bacteria

Compounds	*S. mutans* (μg.mL^{-1})	*S. epidermidis* (μg.mL^{-1})	*P. aeruginosa* (μg.mL^{-1})	*E. coli* (μg.mL^{-1})
L1	512	512	512	512
L2	256	256	256	256
L3	1024	1024	1024	1024
2a	4	4	8	8
2b	2	2	4	4
2c	8	8	8	8
3a	32	32	32	32
3b	16	16	16	16

Values of $p < 0.05$ were considered statistically significant. Prism version 5.0 was used for all statistical analyses.

RESULTS AND DISCUSSION

Formation of the imidazolium salt was manifested by the appearance of imidazolium CH_2 proton at 10.20 ppm in the ^{1}HNMR spectra. The Formation of **L-2** ligand was assigned by the ^{1}HNMR singlet signal at 10.78 ppm and in the case of **L-3,** the same proton appeared at 9.46 ppm which confirmed the formation of the salts. The silver complexes, Chloro [2,6-bis(1-methyl imidazol) pyrazine] silver(I) complex, **2a** and [2,6-bis(1-methyl imidazol)pyrazine silver(I)] hexafluorophosphate complex, **3a** were synthesized by the most convenient reported procedure [17]. The formation of silver complex **2a** and **3a** was ascertained by ^{1}HNMR and ^{13}CNMR spectroscopy. The absence of CH_2 imidazolium proton and 22-34 ppm shift of carbenic carbon in ^{13}CNMR spectra confirmed the formation of **2a** and **3a**. All the NMR data were consistent with the cosister ligand, 2,6-{N-methylimidazolium)pyridinechloride and its silver(I) complex [50]. In the case of **L-3,** the NCHN signal appeared at 140.8 ppm of ^{13}CNMR, and the same carbeneic carbon appeared at 160.4 ppm in the case of **3a**. It is notable that much more carbenic carbon shift was observed in the case of **2a** and **2b** than **3a** and **3b**; this may be due to the presence of two strong σ-donor NHC ligands. The maximum shift at 3 (8) position of aromatic proton in pyrazine was observed in the ^{1}HNMR spectra due to the strong π-acidic characteristics of pyrazine. In the case of **2c,** proton signal of acetate was observed at 1.90 ppm with pyrazine and imidazoline, which confirms the coordination of acetate with silver.

The antibacterial activities of all synthesized compounds were tested against both Gram-positive (*S. mutans* and *S. epidermidis*) and Gram-negative (*P. aeruginosa* and *E. coli*) bacteria. The antibacterial activity of pyrimidine functionalized proligand 1-methyl-3-pyrimidinechloride (**L-1**) and 2,6-bis-[1-methylimidazol-2yl] pyrazinechloride (**L-2**) was tested against both Gram-positive and Gram-negative opportunistic human pathogens. **L-1** required twice the amount of compounds than **L-2** to kill all pathogens and does not exhibit any specificity among. So, it will be interesting to study the antibacterial activity of complexes derived from pro-ligand **L-2** rather than **L-1**. The synthesized compounds, **2a, 2b** and **2c** of proligand **L-2** were tested for their antibacterial efficacy against the same bacterial strains. Interestingly, the MIC values were drastically reduced and mostly effective for Gram-positive bacteria. Pyrazine functionalized Au(I) and Ag(I)-NHC chloride complex showed very low level of MIC value in comparison to acetate complexes. Furthermore, the antibacterial activity of complexes **3a** and **3b** derived from 2,6-bis(1-methyl imidazolium-2yl) pyrazinehexafluorophosphate was less effective than **2a** and **2b** (Table **1**).

Pyrazine functionalized Au(I)-NHC chloride was more active than Ag(I)-NHC chloride salt and Ag(I)-NHC acetate salt complex. In order to determine the effectiveness of complex **2a** and **2b** against MDR pathogens, we used two clinical isolates from humans with antibiotics resistant ability. The isolates were *Staphylococcus aureus*, a Gram-positive cocci and *E. coli,* Gram-negative rod-shaped bacteria. Both the clinically isolated strains are resistant to several classes of antibiotics listed in Table **2**. Several genetic backgrounds are established for resistance to different class of antibiotics such as *aadA* gene cassettes encoding aminoglycoside adenylyltransferases inactivating streptomycin [51], β-lactamase inhibiting ampicillin activity [52], *vanB,* which is responsible for resistance to vancomycin [53], chloramphenicol acetyltransferase, which helps to resist chloramphenicol [54]. There are known mechanisms of fluoroquinolone resistance using efflux pumps, which can act to decrease intracellular quinolone concentration [55]. Thus several mechanisms have evolved in bacteria to develop antibiotic resistance. These mechanisms can chemically modify the antibiotic, render it inactive through efflux pump from the cell, or modify the target site that can then not be recognized by the antibiotic. Synthesized compounds **2a** and **2b** are able to overcome those factors responsible for resistance to selected antibiotics.

Biofilms have been found to be involved in a wide variety of microbial infections in the body and almost 80% of all infections [56]. Hence, efficient biofilm eradication of an antibacterial agent would be a most important factor for the development of future generations of antibiotics. We used the biofilm producing strain, *S. mutans* and *E. coil* to check the usefulness of biofilm eradication ability of compound **2b** and **2a**. Increasing the compound concentration, biofilm was reduced drastically and almost completely eradicated at 8 μg.mL^{-1} concentrations for *E. coli,* whereas eradication of 7 days old biofilm by *S. mutans* grown on

Table 2. Determination of Minimum Inhibitory Concentration (MIC) of Compounds 2a and 2band Choosen Antibiotics Against Two Clinical Isolates. Antibiotics Used were Streptomycin (strp), Ampicillin (Amp), Vancomycin (Vanc), Ciprofloxacin (Cipr) and Chloramphenicol (chlor). The Units of all MIC Values are Represented as μg.mL^{-1}

Bacterial strains	Strp.	Amp.	Vanc.	Cipr.	Chlor.	2a	2b
E. coli	128	64	64	128	16-32	8	4
S. aureus	64	32	32-64	32	64-128	4	2

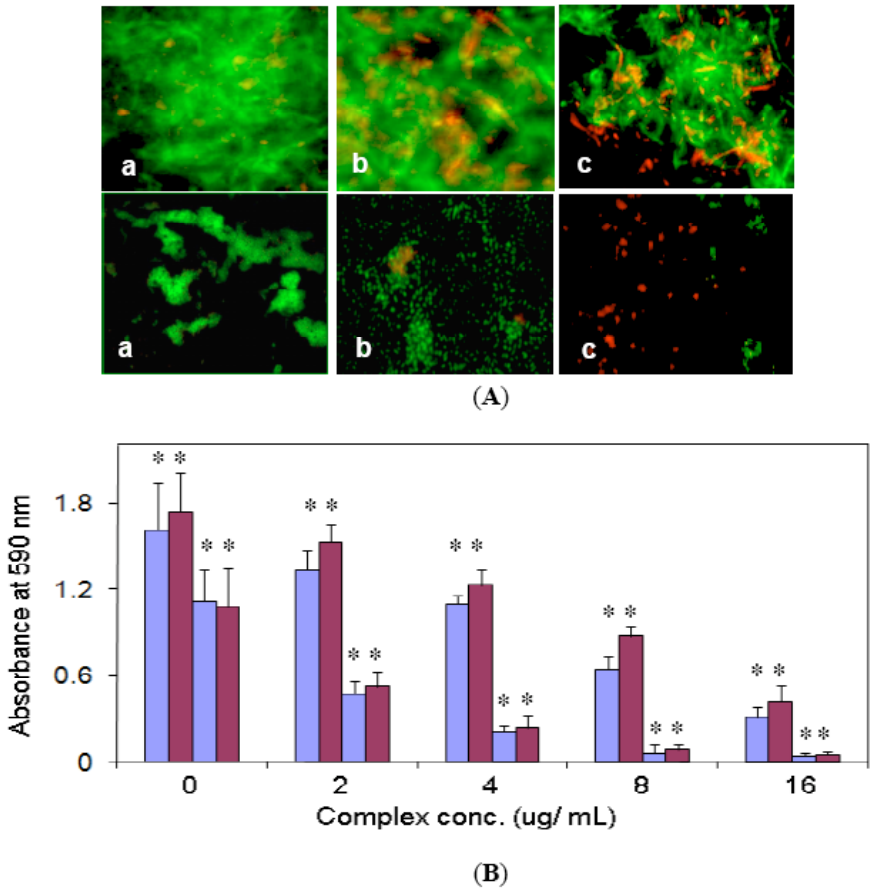

Fig. (1). Effect of compound 2b on the eradication of biofilm formed by bacteria. Images were captured (at 400 magnification) after 24h treatment on biofilm with compound 2b; *S. mutans* biofilm were grown on hydroxyapetite disc coated with human salive (upper panel) and *E.coli* biofilm (lower panel) on polystyrene plate. (**A**). The well containing different concentrations of 2b as 0 μg.mL^{-1} (a); 4 μg.mL^{-1} (b) and 8 μg.mL^{-1} (c). Absorbance (A590) of the crystal violet stained obtained from the biofilm matrix after the treatment with different concentrations of complex 2b (blue colour) and 2a (brick red colour); **B**. Each first two bar data obtained from *S. mutans* biofilm and next two bar data from *E. coli* biofilm. All values were means calculated from three replicate experiments and vertical bars correspond to standard deviations. Different letters represent significant differences between treatments and negative control (0) with $p<0.005$ using one-way ANOVA followed by Dunnett's test.

hydroxyapeptite disc coated with human saliva was delayed (Fig. **1**). The delayed response of the compounds against old biofilm might be due to the effect of huge production exopolymeric network in biofilm that providing a diffusion barrier or directly binds to antimicrobial agents. The modes of antibacterial action of compound **2b** have been evaluated by determining the membrane permeabilization potential on staphylococcal membrane. Flow cytometric analysis was performed to understand the time-dependent internalization potentials of **2b**. Results show that PI fluorescence level was increased by increasing the incubation time with the compounds **2b** (Fig. **2**). An increase in the mean PI fluorescence (red) intensity of 42.50 %, 64.70 %, 77.97 %, 92.33 % and 95.10 % was achieved after 10 min, 20 min, 30 min, 40 min and 60 min incubation periods, respectively. Simultaneously, the live cells' percentage stained with SYTO 9 (green) decreased. Increased red fluorescence level in cells revealed that the membrane permeability increased, allowing the integration of more PI. It also revealed that 40 min time is required to kill > 90% bacterial cells at their MIC concentration level.

Further, the interaction of the bacterial cell wall and **2b** was observed using SEM (Fig. **3**). SEM pictures clearly indicate drastic damage in their cell wall. As a result, membrane permeability of the cells was also increased and the cytoplasmic materials leached out to the environment. Interestingly, the morphology of treated cells revealed a breakdown in their cell wall, which is composed of a peptidoglycan layer. Peptidoglycan is a composition of sugars (β-(1,4), linked N-acetylglucosamine and N-acetylmuramic acid) and tetrapeptide linkage that forms a strong net-like structure at the outside of the plasma membrane. The peptidoglycan layer is thicker in Gram-positive bacteria(20 to 80 nm) than in Gram-negative bacteria (7 to 8 nm) and forms 90% and 10% of the dry weight of Gram-positive and Gram-negative bacteria, respectively. Compounds **2a** and **2b**, both were more active against Gram-positive bacteria than Gram-negative bacteria, correlating with the involvement of the peptidoglycan layer in their target site. The exact mechanism of silver and gold action is still unknown, but both metals have the ability to inhibit the cell division/ reproduction of bacteria [57], and attached to certain receptors they damage microbial membranes, resulting in increased permeability and cell death [58]. Silver and gold react with the amino-, carboxyl-, phosphate-, and imidazole-groups and diminish the activities of lactate dehydrogenase, and glutathione peroxidase, while silver also inactivates the enzymes by reacting with the sulfhydryl groups to form silver sulfides [59]. Moreover, Au(I) has more advantages over other oxidation states of gold, viz., -I, 0, I, II, III, IV; and V; but only gold 0, I, and III are stable in aqueous and biological environments. It was clear from the hemolytic data that it is nontoxic to RBC in the required dose at 2 and 4 µg.mL^{-1} of compound **2b**, which strongly suggests the potential of **2b** to be used as a future antibiotic against antibiotics resistant human

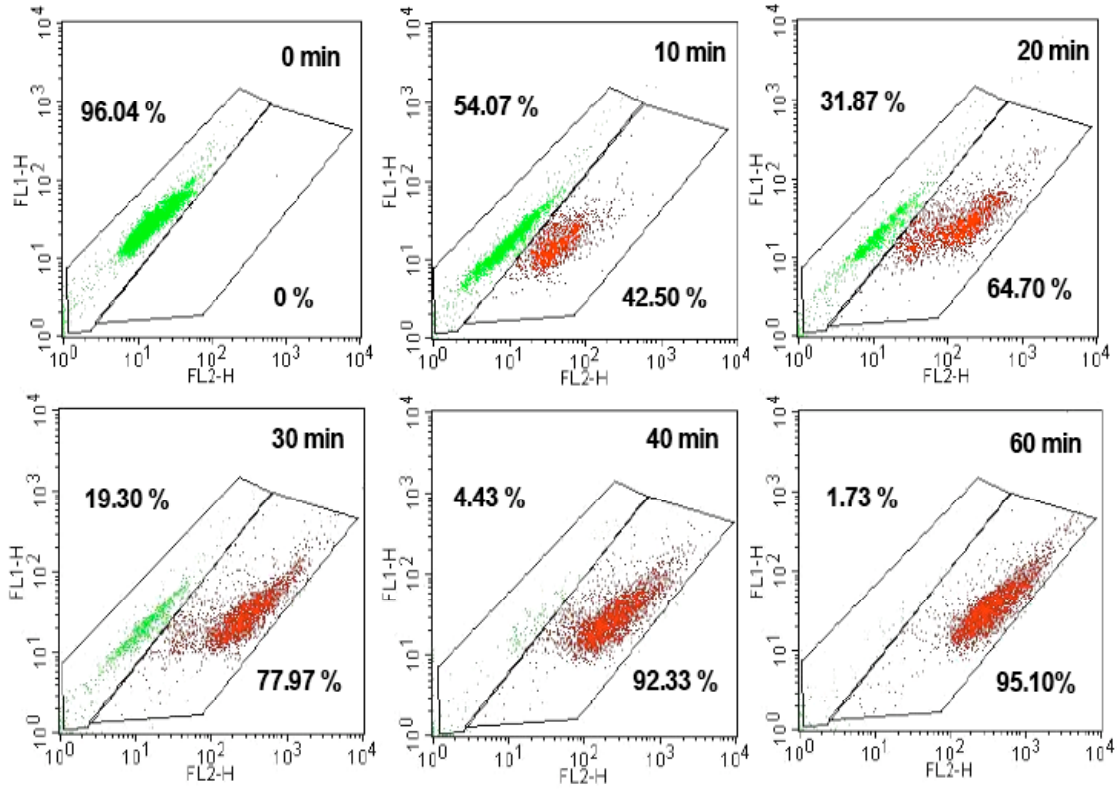

Fig. (2). Determination of staphylococcal membrane permeability and cell viability. S. epidermidis NCIM2493 cells were treated with different concentrations of 2b with fixed concentration of Bacterial Viability Counting Kit for 30 min. Figure shows that red fluorescence (dead cells) intensity increased and green fluorescence (live cells) decreased with increasing time of incubation at fixed concentration of 2b (2 μg.mL^{-1}). A increase in the mean red fluorescence intensity of 42.50 %, 64.70 %, 77.97 %, 92.33 % and 95.10 % was observed at 10 min, 20 min, 30 min, 40 min and 60 min incubation, respectively.

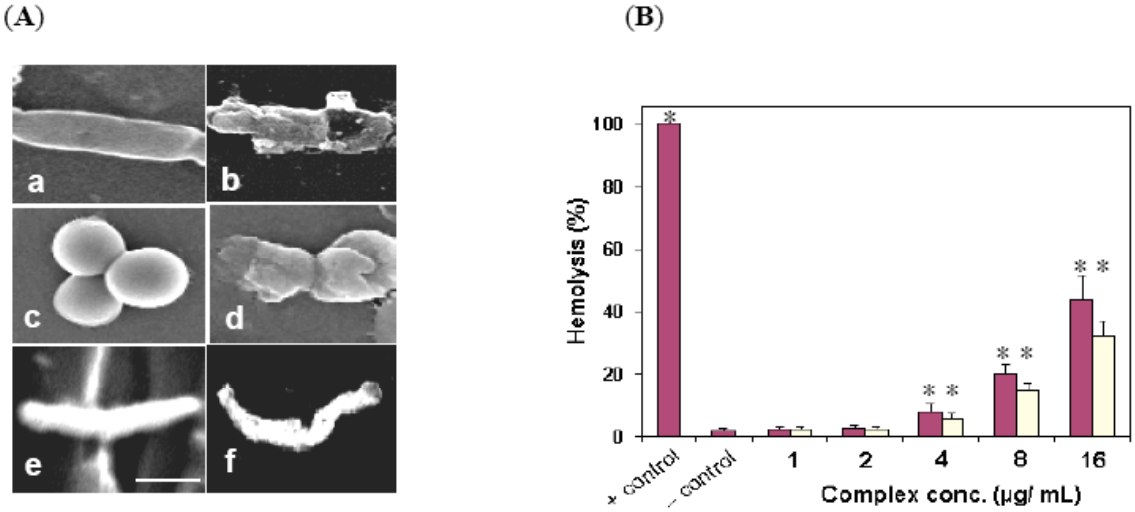

Fig. (3). SEM micrographs of bacteria treated with compound 2b (**A**). All the cells were treated with 2b (4 μg.mL^{-1}) for 40 min at room temperature and the control group was treated with 0.1% DMSO. Control *B. subtilis* cells (a) were treated with 2b (b); Control *S. epidermidis* cells (c) were treated with 2b (d); and Control *P. aeruginosa* cells (e) were treated with 2b (f). Images showed the drastic rupture in cell wall. The image of *B. subtilis* clearly indicates the effect of compounds on cell wall. Hemolytic activity of compound 2b (pink) and 2a (yellow) (**B**). All values were means calculated from three replicate experiments and vertical bars correspond to standard deviations. Asterisks represent significant differences between treatments and negative control with $p<0.005$ using one-way ANOVA followed by Dunnett's test.

pathogens. From the data obtained in this work, it is suggested that the free *N*-atom at L-2 proligand may play a crucial role in the antimicrobial activity. The activity of Au (I)-NHC complexes might be due to the greater stability of the gold-NHC (Au-C) bond than other metal–NHC (M-C) complexes tested here.

Docking results show that the position of **2a** and **2b** changes only when the type of peptidoglycan is changed. Thus, **2a** and **2b** compounds bond to peptidoglycans in the same way, with only a difference in molecular volume, but keeping the same patterns of binding. Considering this, only data related to compound **2b** were

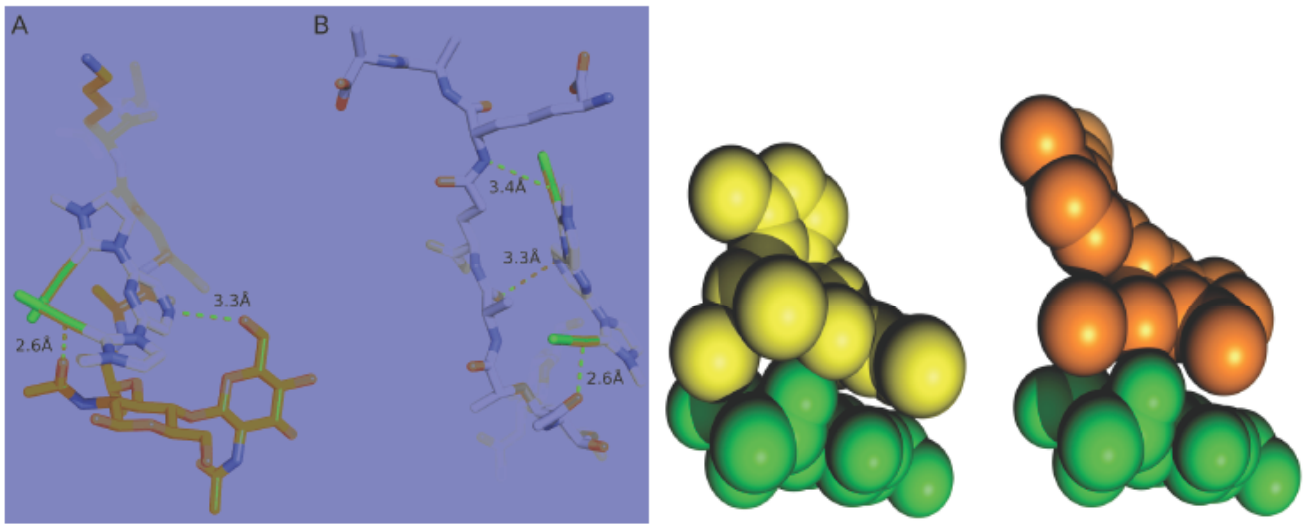

Fig. (4). Theoretical molecular docking of 2b (white backbone) compounds to peptidoglycans. (**A**) 2b docked to Lys-Type peptidoglycan (orange backbone) and (**B**) 2b docked to Dap-Type one (pale blue backbone).2a compound shows similar conformation. Atoms are colored as follow: Oxygen as red; Nitrogen as blue; Gold as gold and Chlorine as green. Carbons are colored as white in 2b; pale blue in Dap-Type peptidoglycan; and orange in Lys-Type one. Hydrogens are hidden for better visualization. Fit of 2b on N-acetylmuramic acid. Docking conformation of 2b to Lys-Type peptidoglycan is displayed in yellow and to Dap-Type one in orange. N-acetylmuramic acid is represented in green. Other atoms were hidden for a better visualization. Molecules are in the same orientation.

shown here (Fig. **4**). Comparing the docking to Lys-Type Peptidoglycan and Dap-Type one, we can observe multiple differences. First, **2b** molecule shows clear backbone torsion when docked to Dap-Type peptidoglycan. Otherwise, when this same compound was docked to Lys-Type peptidoglycan it was not modified compared to free form. Probably, torsion observed in **2b** docked with Dap-Type peptidoglycan may be entailed, due to a modification on surface change in peptidoglycan electrostatic potential. While Lys-Type one has a cationic surface charge due to the presence of a lysine residue, the Dap-Type shows a neutral surface charge, since the positive charge is neutralized by formic acid group, which shows a negative surface (data not shown).

Indeed, **2b** has a greater affinity to Dap-Type peptidoglycan than Lys-Type one. The interaction with Dap-Type one is stabilized by one hydrogen bond formed between O from main chain from Ala2 and the N4 from **2b**. Moreover two electrostatic interactions, between N from Dap and Au33 from **2b** and between O8 from N-acetylmuramic acid (MurNac) and Au34 from **2b** were observed. On the other hand, Lys-Type shows one hydrogen bond between O6 from N-acetylglucosamine and N4 from **2b** and a single electrostatic interaction between O8 from MurNac acid and Au33 from **2b** (Fig. **4**). Moreover, the relative contact area index (RAC) on docking with Dap-Type one (75.85) is lower than Lys-Type one (181.48). This index was considered in order to compare docking results, since no absolute value was obtained. No significant differences were observed between **2a** and **2b**.Thereby, the affinity of **2b** is greater for Dap-Type peptidoglycan; however, Dap-Type is found in Gram-negative bacteria and **2b** is more active against Gram-positive ones. Despite having contrasting data, by analyzing the binding site of **2b** on peptidoglycans, it was observed that the antibiotic compound fits better to MurNac in Lys-Type than Dap-Type one; while in Lys-Type **2b** lies in parallel to MurNac, in Dap-Type it lies in diagonal. These data suggest that **2b** may act to inhibit cell wall formation by blocking the MurNac, inhibiting the polymerization of peptidoglycan, being more efficient against Gram-positive bacteria due to the parallel positioning in relation to MurNac. The greater affinity of **2b** to peptide portion of Dap-Type peptidoglycan restrains it from moving towards MurNac, which leads **2b** to be diagonal in relation to MurNac. The outer membrane of Gram-negative bacteria can also be proposed for preventing **2a** and **2b** to reach the peptidoglycan layer, reducing their activity against Gram-negative bacteria. Vancomicin-derived antibiotics also cause damage to bacterial cell walls. They bind to cell wall precursors on the terminal of the D-Ala-D-Ala dipeptide, inhibiting their processing for peptidoglycan formation60. A similar mechanism of action could also be proposed here. Moreover, simple modification in the vancomycin, such as the modification of a single atom, may modify cell wall precursors of resistant bacteria. It would thus restore antimicrobial activity, showing novel pathways for development of new antibiotics in the treatment of resistant bacterial infections [61]. This was not observed here at molecular levels, since **2a** and **2b** show identical docking patterns. Table **S1** presents the bond lengths and angles of the corresponding complexes which are used for biological assessment. Table **3** depicts the Hardness (η, au), Electronegativity (χ, au),

Table 3. Hardness(η,au), Electronegativity(χ,au), Electrophilicity(ω,au) of Ligands Using Different Basis Sets at B3LYP Level of Theory

Ligands	Basis Sets	η (au)	χ (au)	ω (au)
L-1	6-31+G(d,p)	0.33881	0.31910	0.01725
	6-311+G(d,p)	0.33825	0.32018	0.01734
	6-311++G(d,p)	0.33825	0.32014	0.01733
L-2	6-31+G(d,p)	0.30368	0.42455	0.02737
	6-311+G(d,p)	0.30381	0.42617	0.02759
	6-311++G(d,p)	0.30377	0.42613	0.02758

Electrophilicity (ω, au) of ligands computed at different levels of theory.

From Table **3**, it is evident that **L2** is more reactive and less stable than **L1** which is also found in antibacterial study. As we found that **L2** is more reactive than **L1,** we further investigated the reactivity of different Ag(I) and Au(I) complexes derived from **L2**. This antibacterial study revealed that **2b** is more effective than **2a** and **2c**. This trend is also in good agreement with their relative energy (**2b**>**2a**>**2c**>**3b**>**3a**) (Table **4**). So, the stability order of the complexes are **3a**>**3b**>**2c**>**2a**>**2b**, and the reactivity order will be the reverse. It is clear that the reactivity order of the complexes (**3a**, **3b**, **2a**, **2b** and **2c)** is to be **2b**>**2a**>**2c**>**3b**>**3a,** which also corroborates the antibacterial study.

Table 4. Total Energy (E, au) of Complexes Using B3LYP Level of Theory

Complexes(s)	Besis Set	E (au)
2a	LanL2dz	-1114.40560
2b	LanL2dz	-1093.79914
2c	LanL2dz	-1541.34855
3a	LanL2dz	-1876.79742

In real life systems, complexes are known to interact freely with cellular components when they are in co-planner configuration and have rotational freedom [62a]. Flexible co-planarity [62] is an essential descriptor for the toxicity of the complexes. In the present study, all the five complexes have twisted structure, but among the five **2a**, **2b** and **2c** are flatter than the other two. In the case of **2a**, **2b** and **2c,** the metal centers are bonded with only one ligand (other side attached to Cl atom or –OAc group). So there is a scope for free rotation (at the connectivity of pyrazine and immidazole). This free rotation promotes them to achieve a co-planner configuration within the reaction medium for the easy formation of complexes with cellular components. But for **3a** and **3b,** as the metal centers are connected with two ligands, free rotation is prohibited and the reactivities are less than **2a**, **2b** and **2c.** Docking result also shows that configuration of complexes may change (only where free rotation is possible) depending upon the type of peptidoglycane.

For better understanding, the relative energy of **2a**, **2b** and **2c** are calculated as a function of the tortional angle. We changed the tortional angle for **2a** through the bond N5-C17 up to 170°, for **2b** through the bond N2-C12 up to 170°, for **2c** through the bond N2-C12 up to 150° to have their probable planer conformation. From Fig. (**5**), it is evident that the order of the potential energy barrier is **2a**>**2b**>**2c**. The presence of a large acetate group in **2c** (–OAc) probably restricts the interaction (steric crowding) with peptidoglycan in both its conformers. For **2a** and **2b,** Cl atoms (small w.r.t –OAc) are attached, which favors their free interaction with peptidoglycans. As the potential energy barrier is greater for **2a** (ΔE=14.56Kcal) than **2b** (ΔE=5.90Kcal), **2b** shows better reactivity than **2a**, and **2b** is the most reactive of them all.

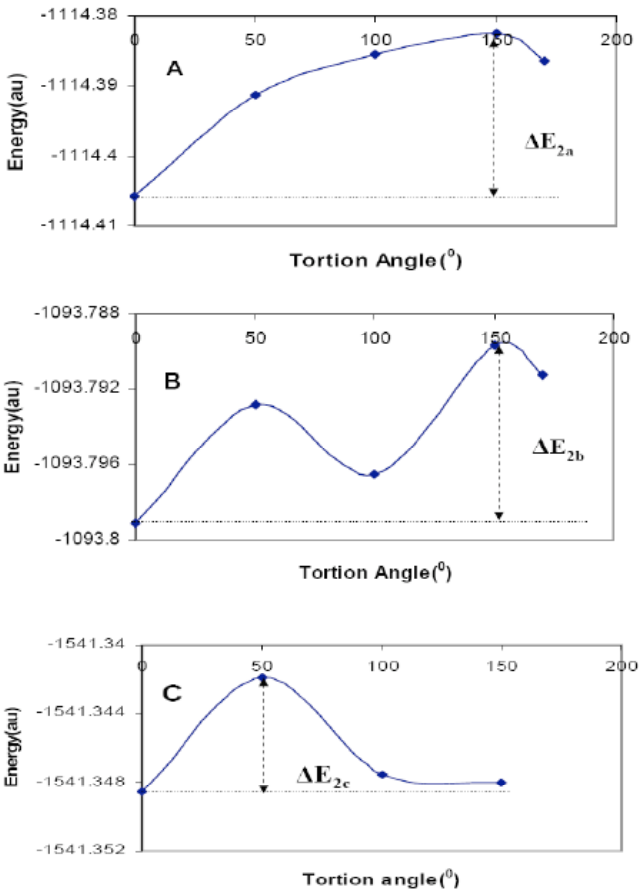

Fig. (5). Potential Energy barrier[(ΔE), indicating the energy difference between the highest and lowest conformers] of the different conformers of the complexes are as a function of the tortional angle. A,B,C are the relative graph of complexes 2a, 2b and 2c. [{ΔE2a =0.023203 au (14.56 Kcal)}, {ΔE2b =0.0.009407 au (5.90 Kcal)}, {ΔE2c =0.00663 au (4.16 Kcal)}].

CONCLUSION

A new series of pyrazine functionalized Ag(I) and Au(I)- NHC complexes were prepared and structurally characterized, and their antibacterial activity with inhibition of biofilm formation was studied. Ligands **L1**, **L2** and **L3** did not exhibit any significant activity, whereas the complex having 2,6-bis(1-methyl imidazol) pyrazinechloride ligand showed better activity compared to other complexes. Chloro [2,6-bis(1-methyl imidazol) pyrazine] gold(I)complex and Chloro [2,6-bis(1-methyl imidazol) pyrazine] silver (I) complex showed potent bactericidal activity against human pathogens that are resistant to several antibiotics, which revealed that the mechanism is different from well established antibiotics' action. It mainly affects the bacterial peptidoglycan layer, composition of cell wall and bacterial membrane. The stability and reactivity of the compounds revealed the strong interaction with negatively charged bacterial cell membrane. Complexes **2b** and **2a** were seen to have the affinity to bind with the peptidoglycan layer, disrupting the cell wall and inhibiting cell wall synthesis. The compounds were less toxic to red blood cells in their minimum inhibitory dose and hence might have potential applications as future antibiotics. In summary, data here reported propose a novel antibiotic compound class and also shed some light on their mechanisms of action, improving the number of effective compounds that could help in infectious bacterial control.

ACKNOWLEDGEMENTS

We would like to gratefully acknowledge Prof. Sujit Roy, School of Basic Science, Indian Institute of Technology Bhubaneswar, Bhubaneswar-751013, India. We wish to express our heartfelt thanks to Dr. Jayangshu Sengupta and Suman Saha, Priyamvada Birla Aravind Eye Hospital, 10, Loudon Street, Kolkata-700 017, W B, India for providing the necessary facilities of clinical study. JD thanks the Department of Science and Technology, India, for financial support.

CONFLICT OF INTEREST

None declared.

ABBREVIATIONS

NHCs = *N*-heterocyclic carbenes

CLSI = clinical and laboratory standards institute

CDFT = conceptual density functional theory

MHB = Mueller-Hinton broth

TSB = trypticase soy broth

MIC = minimum inhibitory concentration

L-1 = 2-(1-methylimidazolium) pyrimidinechloride

L-2 = 2,6-bis(1-methyl imidzol)pyrazinechloride

2a = chloro [2,6-bis(1-methyl imidazol)pyrazine]silver(I) complex

2b = chloro [2,6-bis(1-methyl imidazol)pyrazine]gold(I)complex

2c = acetato [2,6-bis(1-methyl imidazol)- pyrazine]silver(I) complex

3a = 2,6-bis(1-methyl imidazol)-pyrazinesilver(I)]hexafluorophosphate complex

3b = 2,6-bis(1-methyl imidazol)pyrazine-gold(I)]hexafluorophosphate complex

REFERENCES

[1] Sharma, A. Antimicrobial resistance: No action today, no cure tomorrow. *Ind. J. Med. Microbiol.* **2011**, 29, 91-92.

[2] Bourissou, D.; Guerret, O.; Gabbai F. P.; Bertrand, G. Stable Carbenes. *Chem. Rev.* **2000**, 100, 39-91.

[3] de Fremont, P.; Marion, N.; Nolan, S. P. Carbenes: Synthesis, properties, and organometallic chemistry. *Coord. Chem. Rev.* **2009**, 253, 862-893.

[4] Canac Y.; Soleilhavoup M.; Conejero S.; Bertrand G.J. Stable non-N-heterocyclic carbenes (non-NHC): recent progress. *J. Organomet. Chem.* **2004**, 689, 3857-3865.

[5] Melaimi M.; Soleilhavoup M.; Bertrand G. Stable cyclic carbenes and related species beyond diaminocarbenes. *Angew. Chem. Int. Ed.* **2010**, 49, 8810-8849.

[6] Schuster O.; Yang L.; Raubenheimer H. G.; Albrecht M. Beyond conventional N-heterocyclic carbenes: abnormal, remote, and other Classes of NHC ligands with reduced heteroatom stabilization. *Chem. Rev.* **2009**, 109, 3445-3478.

[7] Ofele K.; Tosch E.; Taubmann C.; Herrmann W. A.; Carbocyclic carbene metal complexes. *Chem. Rev.* **2009**, 109, 3408-3444.

[8] Wanzlick H. W. Aspects of nucleophilic carbene chemistry. *Angew. Chem. Int. Ed. Engl.* **1962**, 1, 75-80.

[9] Wanzlick H. W.; Sch€onherr H. J. Direct synthesis of a mercury salt-carbene complex. *Angew. Chem, Int. Ed. Engl.* **1968**, 7, 141-142.

[10] Arduengo A. J. III ; Harlow R. L. ; Kline M. A. A Stable crystalline carbene. *J. Am. Chem. Soc.* **1991**, 113, 361-363.

[11] Peris E.; Crabtree R.H. Recent homogeneous catalytic applications of chelate and pincer N-heterocyclic carbenes. *Coord. Chem. Rev.* **2004**, 248, 2239-2246.

[12] Crudden C. M.; Allan D.P. Stability and reactivity of N-heterocyclic carbene complexes. *Coord. Chem. Rev.* **2004**, 248, 2247-2273.

[13] Puch D.; Danopoulos A. A. Metal complexes with 'pincer'-type ligands incorporating N-heterocyclic carbene functionalities. *Coord. Chem. Rev.* **2007**, 251, 610-641.

[14] Adhikary S. D.; Samanta T.; Roymahapatra G.; Loiseau F.; Jouvenot D.; Dinda J. Synthesis, structure and electrochemical behaviour of Ru(II)- and Pt(II)-carbene complexes of the NCN-pincer1,3-bis(2-pyridylmethyl)-1H-benzimidazolium chloride. *New J. Chem.* **2010**, 34, 1974-1980.

[15] Hahn F. E.; Jahnke M. C.; Heterocyclic carbenes: synthesis and coordination chemistry. *Angew. Chem.* **2008**, 47, 3122–3172.

[16] Marion N.; González S. D.; Nolan S. P. N-heterocyclische carbene also organokatalysatoren. *Angew. Chem.* **2007**, 119, 3046-3058.

[17] Wang H. M. J.; Lin I. J. B. Facile synthesis of silver(I)-carbene complexes. Useful carbene transfer agents. *Organometallics*. **1998**, 17, 972-975.

[18] Russel, A. D.; Path, F. R.; Hugo, W. B.; Antimicrobial activity and action of silver. *Prog. Med. Chem.* **1994**, 31, 351-370.

[19] Landsdown, A. B. G.. A review of the use of silver in wound care: facts and fallacies. *Br. J. Nursing.* **2004**, 13, S6-S19.

[20] Landsdown, A. B. G. Bacterial resistance to silver in wound care and medical devices. *J. Wound Care*. **2007**, 16, 15-19.

[21] Blodgett, R. C.; Heuer, M. A.; Pietrusko, R. G. Auranofin: a unique oral chrysotherapeutic agent. *Semin. Arth. Rheum.* **1984**, 255-273.

[22] Chaffman, M.; Brogden, R. N.; Heel, R. C.; Speight, T. M. ; Avery, G. S. Auranofin. A preliminary review of its pharmacological properties and therapeutic use in rheumatoid *Arthritis. Drugs*. **1984**, 27, 378-424.

[23] McKeage, M. J.; Maharaj, L.; Berners-Price, S. J. Mechanisms of cytotoxicity and antitumor activity of gold(I) phosphine complexes: the possible role of mitochondria. *Coord. Chem.Rev.* **2002**, 232 ,127-135.

[24] Rigobello, M. P.; Scutari, G.; Folda A.; Bindoli A. Mitochondrial thioredoxin reductase inhibition by gold(I) compounds and concurrent stimulation of permeability transition and release of cytochrome c. *Biochem. Pharmacol.* **2004**, 67, 689-696.

[25] Rigobello, M. P.; Scutari, G.; Boscolo, R.; Bindoli, A. Induction of mitochondrial permeability transition by auranofin, a gold(I)-phosphine derivative. *Br. J. Pharmacol.* **2002**, 136, 1162-1168.

[26] Lillo, V.; Mas-Marzá, E.; Segarra, A. M.; Carbó, J. J.; Bo, C.; Peris, E.; Fernandez, E. Palladium-NHC complexes do catalyse the diboration of alkenes: mechanistic insights *Chem. Commun.* **2007**, 3380-3382.

[27] Loch, J. A.; Albrecht, M.; Peris, E.; Mata, J.; Faller, J. W.; Crabtree, R. H. Palladium complexes with tridentate pincer bis-carbene ligands as efficient catalysts for C–C coupling. *Organometallics*, **2002**, 21, 700-706.

[28] Stephan, M.; Goetz, B.; Richard, F.; Tobias, S. Patent No. DE102008022788, Application No. DE2008-102008022788, Dated. 2008-05-08.

[29] Hindi, K. M.; Panzner, M. J.; Tessier, C. A.; Cannon, C. L.; Youngs, W. J. The Medicinal Applications of Imidazolium Carbene–Metal Complexes. Chem. Rev. 2009, 109, 3859-3884.

[30] Panzner, M. J.; Hindi, K. M.; Wright, B. D.; Taylor, J. B.; Han, D. S.; Youngs, W. J.; Cannon, C. L. A theobromine derived silver N-heterocyclic carbene: synthesis, characterization, and antimicrobial efficacy studies on cystic fibrosis relevant pathogens. *Dalton Trans.* **2009**, 35, 7308-7313.

[31] Patil, S.; Deally, A.; Gleeson, B.; Müller-Bunz, H.; Paradisi, F.; Tacke, M. Novel benzyl-substituted N-heterocyclic carbene–silver acetate complexes: synthesis, cytotoxicity and antibacterial studies. Metallomics. **2011**, 3, 74-88.

[32] Hindi, K.M.; Siciliano, T. J.; Durmus, S.; Panzner, M. J.; Medvetz, D. A.; Reddy, D. V.; Hogue, L. A.; Hovis, C. E.; Hilliard, J. K.; Mallet, R. J.; Tessier, C. A.; Cannon, C. L.; Youngs, W. J. Synthesis, stability, and antimicrobial studies of electronically tuned silver acetate N-Heterocyclic carbenes. J. Med. Chem. **2008**, 51, 1577-1583.

[33] Samantaray, M. K.; Katiyar, V.; Pang, K.; Nanavati, H.; Ghosh, P. Silver N-heterocyclic carbene complexes as initiators for bulk ring-opening polymerization (ROP) of l-lactides. J. *Organometallic Chem*. **2007**, 692, 1672-1682.

[34] Clinical and Laboratory Standards Institute Performance standards for antimicrobial susceptibility testing. Seventeenth informational supplement Document M100-S17. CLSI, Wayne, PA: CLSI. 2007.

[35] Mandal, S. M.; Pati, B. R.; Das, A. K.; Ghosh, A. K. Characterization of a symbiotically effective *Rhizobium* resistant to arsenic: Isolated from the root nodules of *Vigna mungo* (L.) Hepper grown in an arsenic-contaminated field. *J. Gen. Appl. Microbiol.* 54, **2008**, 93-99.

[36] Croes, S.; Deurenberg, R. H.; Boumans, M. L.; Beisser, P. S.; Neef, C.; Stobberingh E. E. *Staphylococcus aureus* biofilm formation at the physiologic glucose concentration depends on the *S. aureus* lineage. *BMC Microbiol.* **2009**, 9, 229.

[37] Coenye, T.; Honraet, K.; Rigole, P.; Nadal Jimenez, P.; Nelis, H. J. *In vitro* Inhibition of *Streptococcus mutans* Biofilm Formation on Hydroxyapatite by Subinhibitory Concentrations of Anthraquinones. *Antimicrob. Agents Chemother*. **2007**, 51, 1541.

[38] Jarosz, L. M.; Deng, D. M.; van der Mei, H. C.; Crielaard, W.; Krom, B. P. *Streptococcus mutans* competence-stimulating peptide inhibits *Candida albicans* hypha formation. *Eukaryot. Cell*. **2009**, 8, 1658.

[39] Olson, M. E.; Ceri, H.; Morck, D. W.; Buret, A. G.; Read, R. R. Biofilm bacteria: formation and comparative susceptibility to antibiotics. *Can. J. Veter. Res*. **2002**, 66, 86.

[40] Mandal, S. M.; Migliolo, L.; Franco, O. L.; Ghosh, A. K. Identification of an antifungal peptide from *Trapa natans* fruits with inhibitory effects on *Candida tropicalis* biofilm formation. *Peptides*. **2011**, 32, 1741.

[41] Parr, R. G.; Donnelly, R. A.; Levy, M.; Palke, W. E. Electronegativity: The density functional viewpoint. *J. Chem. Phys.* **1978**, 68, 3081-3807.

[42] (a)Parr, R. G.; Pearson, R. G.. Absolute hardness: companion parameter to absolute electronegativity. *J. Am. Chem. Soc.* **1983**, 105, 7512-7516. (b) Pearson, R. G. Chemical Hardness: Applications from Molecules to Solids; Wiley-VCH: Weinheim, 1997.

[43] (a) Chattaraj, P. K., Sarkar, U.; Roy, D. R. Electrophilicity Index. *Chem. Rev.* **2006**, 106, 2065-2091;(b) Chattaraj, P. K.; Roy, D. R. Update 1 of: Electrophilicity Index. *Chem. Rev.* **2007**, 107, PR46-PR74; (c) Chattaraj, P. K.; Giri, S.; Duley, S. Update 2 of: Electrophilicity Index. *Chem. Rev.* **2011**, 111, PR43-PR75.

[44] Gaussian 03, Revision E.01; Gaussian, Inc., Wallingford CT, 2004.

[45] Parthasarathi, R.; Padmanabhan, J.; Subramanian, V.; Maiti, B.; Chattaraj, P. K. Chemical reactivity profiles of two selected polychlorinated biphenyl. *J. Phys. Chem. A* **2003**, 107, 10346-10352. (70a) Arulmozhiraja, S.; Selvin, P. C.; Fujiti, T. Structures, potential energy curves, and torsional barrier heights for selected polychlorinated biphenyls: A Density Functional Theory Study. *J. Phys. Chem. A*. **2002**, 106, 12376-12385.

[46] Cho, S.; Wang, Q.; Swaminathan, C. P.; Hesek, D.; Lee, M.; Boons, G.. J.; Mobashery, S.; Mariuzza, R. A. Structural insights into the bactericidal

mechanism of human peptidoglycan recognition proteins. *Proc. Natl. Acad. Sci. U S A*. **2007**, 104, 8761.

[47] Delano Scientific, LLC .The PyMol molecular graphics system, Version 1.2. http://www.pymol.org.

[48] Trott, O.; Olson, A. J. AutoDock Vina: improving the speed and accuracy of docking with a new scoring function, efficient optimization, and multithreading. *J Comput. Chem.* **2010**, 31, 455-461.

[49] Morris, G.. M.; Huey, R.; Lindstrom, W.; Sanner, M. F.; Belew, R. K.; Goodsell, D. S.; Olson, A. J. AutoDock4 and AutoDockTools4: Automated docking with selective receptor flexibility. *J Comput Chem.* **2009**, 30, 2785-2791.

[50] (a) Peris, E.; Loch, J. A..; Mata, J.; Crabtree, R. H.; A Pd complex of a tridentate pincer CNC bis-carbene ligand as a robust homogenous Heck catalyst, *Chem. Commun.* **2001**, 201-202. (b) Nielsen, D. J.; Cavell, K. J.; Skelton, B. W.; White, A. H.; *Inorg. Chim. Acta.* **2002**, 327, 116-125.

[51] Recchia, G.. D.; Hall, R. M. Gene cassettes: a new class of mobile element. *Microbiology*, **1995**, 141, 3015-3027..

[52] Briñas, L.; Zarazaga, M.; Sáenz, Y.; Ruiz-Larrea, F.; Torres, C. Beta-lactamases in ampicillin-resistant *Escherichia coli* isolates from foods, humans, and healthy animals. Antimicrob. Agents Chemother. **2002**, 46, 3156-3163.

[53] Evers, S.; Courvalin, P. Regulation of VanB-type vancomycin resistance gene expression by the VanS(B)-VanR (B) two-component regulatory system in *Enterococcus faecalis* V583. *J Bacteriol.* **1996**, 178,1302-1309.

[54] Shaw, W.V.; Bentley, D.W.; Sands, L. Mechanism of chloramphenicol resistance in *Staphylococcus epidermidis*. *J. Bacteriol.* **1970**, 104, 1095-1105.

[55] Morita, Y.; Kodama, K.; Shiota, S.; Mine, T.; Kataoka, A.; Mizushima, T.; Tsuchiya T. NorM, a putative multidrug efflux protein, of *Vibrio parahaemolyticus* and its homolog in *Escherichia coli*. *Antimicrob. Agents Chemother.* **1998**, 42, 1778-1782.

[56] Research on microbial biofilms (PA-03-047, NIH , National Heart Lung and Blood Institute. **2002**, 12.

[57] Li, W. R.; Xie, X. B.; Shi, Q. S.; Zeng, H. Y.; Ou-Yang, Y. S.; Chen, Y. B. Antibacterial activity and mechanism of silver nanoparticles on *Escherichia coli*. *Appl. Microbiol. Biotechnol.* **2009**, 85, 1115-1122.

[58] Sondi, I.; Salopek-Sondi, B. Silver nanoparticles as antimicrobial agent: a case study on E. coli as a model for Gram-negative bacteria. *J. Colloid Interface Sci.* **2004**, 275, 177-182.

[59] Fung, M. C.; Bowen, D. L. Silver products for medical indications: risk-benefit assessment. *J Toxicol. Clin. Toxicol.* **1996**, 34, 119-126.

[60] Ge, M.; Chen, Z.; Onishi, H. R.; Kohler, J.; Silver, L. L.; Kerns, R.; Fukuzawa, S.; Thompson, C.; Kahne, D. Vancomycin derivatives that inhibit peptidoglycan biosynthesis without binding D-Ala-D-Ala., D-Ala-D-Ala. *Science*. **1999**, 284, 507-511.

[61] Xie, J.; Pierce, J. G.; James, R. C.; Okano, A.; Boger, D. L. A Redesigned vancomycin engineered for dual d-Ala-d-Ala and d-Ala-d-Lac binding exhibits potent antimicrobial activity against vancomycin-resistant bacteria. *J. Am. Chem. Soc.*, **2011**, 133, 13946-13949.

[62] Parthasarathi, R. ; Padmanabhan, J. ; Subramanian, V.; Maiti, B.; Chattaraj, P. K. J. Phys. Chem. A 2003, 107, 10346. (60a) Arulmozhiraja, S.; Selvin, P.C.; Fujiti, T. J. Phys. Chem. A 2002, 106, 1765.